Measurements of OH and RO2 radicals at the coastal Antarctic site of Dumont d'Urville (East Antarctica) in summer 2010-2011

Alexandre Kukui, Michel R. Legrand, Gérard Ancellet, Valérie Gros, Slimane Bekki, Roland Sarda-Estève, Rodrigue Loisil, Suzanne Preunkert

Measurements of OH and RO$_2$ radicals at the coastal Antarctic site of Dumont d'Urville (East Antarctica) in summer 2010–2011

A. Kukui,[1] M. Legrand,[2] G. Ancellet,[1] V. Gros,[3] S. Bekki,[1] R. Sarda-Estève,[3] R. Loisil,[4] and S. Preunkert[2]

[1]   Measurements of OH and total peroxy RO$_2$ (HO$_2$ plus organic peroxy) radicals were conducted in December 2010/January 2011 at the coastal East Antarctic site of Dumont d'Urville (DDU, 66°40′S 140°01′E) as part of the Oxidant Production over Antarctic Land and its Export (OPALE) project. Compared to measurements carried out at the West Antarctic coast, relatively high concentrations of radicals were found with 24 h average values of 2.1×10^6 and 3.3×10^8 molecule cm^{-3} for OH and peroxy radicals, respectively. On the basis of the steady state calculations, the observed high concentration of peroxy radicals is in good agreement with the observed levels of O$_3$ and HCHO representing via their photolysis the major primary radical sources. The observed OH levels at DDU could be explained only assuming some RO$_2$ to OH conversion mechanism equivalent to the presence of NO in the range of 10 to 50 pptv. As neither NO nor halogen oxides were measured at DDU the mechanism of this recycling could not be explicitly identified. However, an examination of variability of radical levels as a function of the origin (oceanic versus continental) of sampled air masses suggests a more important OH production from RO$_2$ recycling in continental air masses.

Citation: Kukui, A., M. Legrand, G. Ancellet, V. Gros, S. Bekki, R. Sarda-Estève, R. Loisil, and S. Preunkert (2012), Measurements of OH and RO$_2$ radicals at the coastal Antarctic site of Dumont d'Urville (East Antarctica) in summer 2010–2011, *J. Geophys. Res.*, *117*, D12310, doi:10.1029/2012JD017614.

1. Introduction

[2]   During the last decades the interest to the atmospheric chemistry in Antarctica has significantly grown, partly driven (see arguments in S. Preunkert et al., Oxidant Production over Antarctic Land and its Export (OPALE) project: An overview of the 2010–2011 summer campaign, submitted to *Journal of Geophysical Research*, 2012) by the need to better understand key biogeochemical cycles of these regions such as the sulfur cycle. One of the major finding of the last decade was to realize that the photolysis of HNO$_3$ present in snow acts as a source of NO$_x$ (NO+NO$_2$) during the austral summer [*Honrath et al.*, 1999, 2000; *Jones et al.*, 2001], resulting in an unexpected intense photochemical activity in the overlying atmosphere of this remote region. Unexpectedly high levels of NO (up to 600 pptv), and of OH radicals (24 h average value of 2.5×10^6 molecule cm^{-3}), have been first observed at the South Pole as part of the ISCAT studies in 1998–1999 [*Mauldin et al.*, 2001] and then confirmed in more recent studies (ANTCI 2003) [*Mauldin et al.*, 2010]. These findings were explained by strong surface snow emissions of NO$_x$ and the existence of a shallow boundary layer resulting in high NO levels. As a consequence a fast recycling of HO$_2$ radicals via reaction with NO leads to the elevated OH concentrations [*Davis et al.*, 2001]. However, the extrapolation of the South Pole findings at the scale of the Antarctic plateau is not straightforward, as discussed in several studies (ANTCI 2003 [*Wang et al.*, 2007] and ANTCI 2005 [*Slusher et al.*, 2010]).

[3]   First studies conducted at the Antarctic coast revealed a rather low photochemical activity in these regions. In the pioneering study conducted in 1994 at Palmer Station situated in the west Antarctic Peninsula (64°46′S, 64°03′W), relatively low OH concentrations were observed, noon maximum value of 9×10^5 molecule cm^{-3} on clear days [*Jefferson et al.*, 1998]. These data were consistent with estimated low NO levels (close to 5 pptv) and observed O$_3$ mixing ratios (9–20 ppbv). Similarly low OH levels, mean noon maximum value of 7.9×10^5 molecule cm^{-3}, were observed in 2005 at Halley Station also located at the west coast of Antarctica (75°35′S, 26°39′W) (CHABLIS) [*Bloss et al.*, 2007]. At that site ozone levels were rather low (2.6–10.5 ppbv [*Bloss et al.*, 2007]). The radical levels observed during CHABLIS could not be reproduced by model accounting for the observed halogen oxides levels (3.3 pptv of IO and 2.5 pptv of BrO), simulations

---

[1]Laboratoire des Atmosphères, Milieux, Observations Spatiales, Guyancourt, France.

[2]Laboratoire de Glaciologie et Géophysique de l'Environnement, St Martin d'Hères, France.

[3]Laboratoire des Sciences du Climat et de l'Environnement, Gif sur Yvette, France.

[4]Division Technique, INSU, Meudon, France.

Corresponding author: A. Kukui, Laboratoire des Atmosphères, Milieux, Observations Spatiales, 11 Boulevard d'Alembert, FR-78280 Guyancourt, France. (kukui@latmos.ipsl.fr)

Table 1. Comparison of Various Parameters Observed at Antarctic Sites Where Measurements of Radicals are Available[a]

	Site			
	DDU	Halley	Palmer	South Pole
Scientific project	OPALE	CHABLIS	SCATE	ISCAT 2000
Referenced study	This study	*Bloss et al.* [2010]	*Jefferson et al.* [1998]	*Chen et al.* [*Chen et al.*, 2007, and references therein]
Period	26.12.2010–14.01.2011	Jan 2005–Feb 2005	Feb 1994	15.11.2000–30.12.200
Mean air temperature, K	272.5	268		247
Longitude	66°67′S	75°35′S	64°46′S	90°S
Latitude	140°0′E	26°19′E	64°03′E	
OH, 10^6 molecule cm^{-3}	2.1 (<LOD - 6.2)	0.39 (<LOD - 2.8)	0.1 (<0.1–0.9)	2.5 (0–4)[b]
OH noon[c] (10^6 molecule cm^{-3})	3.3	0.79	0.7	
RO$_2$, 10^8 molecule cm^{-3}	3.3 (0.14–6.6)	0.23 (<LOD – 1.1)[d]		0.7 (0.5–1)[b]
J(O^{1}D), 10^{-5} s^{-1}	1.1 (<LOD - 4.3)[e]	1.5 (0.0046–5.9)		0.72 (0.4–1.11)
J(NO$_2$), 10^{-2} s^{-1}	0.6 (<LOD - 1.9)[e]	0.94 (0.044–2.36)		0.99 (0.6–1.25)
O$_3$, ppbv	21 (12–38)[f]	7 (2.6–10.5)	(9–20)	32 (17–51)
H$_2$O	9×10^{16} cm^{-3}	9.4×10^{16} cm^{-3}		0.067%
NO pptv	(5–70) (estimated)	7.3 (<LOD - 42.6)	5 (estimated)	103 (2–570)
HONO, pptv		7 (<LOD – 38)		26 (12–33)
CO, ppbv	40[g]	34.4	(70–90)	37
HCHO, pptv	167 (70–498)[f]	127 (<LOD – 385)		100 (20–170)
CH$_3$CHO, pptv	305 (24–2140)[f]			
H$_2$O$_2$, pptv	380 (145–1000)[f]	79[g]		260 (30–560)
CH$_3$OOH range, pptv	260 (75–550)[f]			
H$_2$, ppbv	400[h]	546		
NH$_3$, ppbv	(0–40)[f]			
DMS, pptv	55[f]			

[a]If not assigned different, average and ranges (in parentheses) are given.
[b]*Mauldin et al.* [2004].
[c]Median value between 10:00–14:00 local time.
[d]HO$_2$ concentration (RO$_2$ was not measured).
[e]Calculated in this work.
[f]*Preunkert et al.* (submitted manuscript, 2012).
[g]*Walker et al.* [2006].
[h]Estimation based on the measurements at DDU using GC analyzer fitted with a HgO.

systematically over-predicting OH and HO$_2$ levels by a factor of 3 to 4 [*Bloss et al.*, 2010].

[4] Studies of oxidants at the East Antarctic coast are scarcer. Relatively high O$_3$ levels were however found at Dumont d'Urville (DDU) in summer by *Legrand et al.* [2009] suggesting a more significant influence of the inland Antarctic air masses reaching that site. More efficient NO$_x$ transport from the high plateau to the East Antarctic coast and hence higher NO$_x$ levels over East Antarctica were also predicted by a 3-D model using a parameterization of NO$_x$ emissions [*Wang et al.*, 2007].

[5] The need to characterize the oxidative capacity of the atmosphere in the vast region of East Antarctica motivated the OPALE (Oxidant Production over Antarctic Land and its Export) initiative (Preunkert et al., submitted manuscript, 2012). The objective of the first phase of the OPALE project conducted at the site of DDU was to characterize the oxidative capacity of the atmosphere at the coast of East Antarctica and to evaluate to what extent this region is influenced by the outflow of continental air from the high east Antarctic plateau. In this framework we present here first measurements of OH and total peroxy RO$_2$ (HO$_2$ + organic peroxy) radicals carried out in December 2010/January 2011 at DDU.

2. Experimental Setup

2.1. Campaign Description

[6] The radical measurements were performed from 26 December 2010 to 14 January 2011 at the "iono" site located at the southern side of the "Ile des Pétrels" island, about 500 m away from the main DDU station. As discussed by Preunkert et al. (submitted manuscript, 2012), the record of CO shows that the "iono" site was sometimes impacted by station activities but these events remained limited to less than one hour. The "Ile des Pétrels" and other surrounding small islands are occupied by large penguin colonies that emit large amount of ammonia [*Legrand et al.*, 1998] through the bacterial decomposition of deposits (uric acid). *Legrand et al.*, 2012 demonstrated that in addition to ammonia several oxygenated volatile organic compounds including mainly acetic acid, acetaldehyde, and acetone are emitted by this local source.

[7] The whole field chemical measurements program is detailed in Preunkert et al. (submitted manuscript, 2012) and we summarized in Table 1 concentration means and ranges for species relevant for discussion of OH and RO$_2$ sources and sinks. They include ozone, CO, NH$_3$, aldehydes (HCHO, CH$_3$CHO), hydroperoxides (H$_2$O$_2$, CH$_3$OOH), acetic acid, acetone, and DMS as well as basic meteorological parameters (temperature, pressure, humidity, and wind conditions). Planned measurements of NO and NO$_2$ were not possible due to logistic problems caused by a tragic helicopter accident (Preunkert et al., submitted manuscript, 2012).

[8] Following a breakdown of the actinic flux radiometer, neither photolysis rates nor actinic fluxes were available during the DDU field campaign. The values of the photolysis rates needed to discuss radical data have been therefore
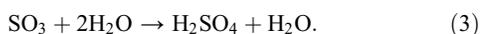
Figure 1. Arrangement for measurements of OH and RO$_2$ radicals at DDU.

estimated from measurements of the global UV-B erythemal irradiance and total global irradiance routinely monitored at DDU. Detailed description of the approach used for this estimation is presented in Appendix A. The estimated uncertainties for solar zenith angle less than 75° are 20% and 25% for J(O^{1}D) and J(NO$_2$), respectively. These uncertainties result from error on the estimated albedo value (0.6 ± 0.1) and the 2σ measurement uncertainties. The uncertainty of the photolysis rates of other relevant species (HONO, HCHO, CH$_3$CHO, H$_2$O$_2$ and CH$_3$OOH) is estimated to be of 30%.

2.2. Radical Measurement Technique

[9] The radicals OH, RO$_2$ (the sum of hydroperoxy HO$_2$ and organic peroxy radicals) and sulfuric acid (not shown) have been measured using chemical ionization mass spectrometry (CIMS) [*Eisele and Tanner*, 1991; *Berresheim et al.*, 2000]. Detailed description of the instrument has been presented elsewhere [*Kukui et al.*, 2008]. Here we briefly present the principle of the method and report details on the setup of the device and applied working conditions during the OPALE campaign.

[10] The OH radical was measured by titrating sampled OH radicals into H$_2$SO$_4$ by addition of SO$_2$ into a chemical conversion reactor in the presence of water vapor and oxygen [*Eisele and Tanner*, 1991; *Tanner et al.*, 1997; *Berresheim et al.*, 2000], according to the following reactions:

$$OH + SO_2 + M \rightarrow HSO_3 + M \tag{1}$$

$$HSO_3 + O_2 \rightarrow SO_3 + HO_2 \tag{2}$$

$$SO_3 + 2H_2O \rightarrow H_2SO_4 + H_2O. \tag{3}$$

[11] H$_2$SO$_4$ was detected by using mass spectrometry as HSO$_4^-$ ion produced by chemical ionization with NO$_3^-$ in an ion-molecule reactor following the chemical conversion reactor:

$$H_2SO_4 + NO_3^- \rightarrow HSO_4^- + HNO_3 \tag{4}$$
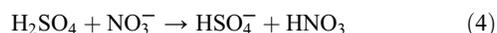
[12] To account for the contribution of atmospheric sulfuric acid the chemical conversion was performed using isotopically labeled ^{34}SO$_2$ leading to the formation of H$_2$^{34}SO$_4$.

[13] The concentration of total peroxy radicals (RO$_2$) was measured by converting them into OH radicals via reactions with NO [*Reiner et al.*, 1997] (reactions (5) to (7)), hereafter converted into sulfuric acid:

$$RO_2 + NO \rightarrow RO + NO_2 \tag{5}$$

$$RO + O_2 \rightarrow R'O + HO_2 \tag{6}$$

$$HO_2 + NO \rightarrow OH + NO_2. \tag{7}$$

[14] During the measurements the instrument was set up in a container with the chemical conversion reactor protruded through an interface cap covered with a Teflon sheet and fixed on the roof of the container (Figure 1). The sampling aperture of the reactor (3 mm diameter) was placed 50 cm above the roof (i.e., about 4 m above the ground). The reactor is similar to the one described in *Kukui et al.* [2008] except that the modified reactor is made of stainless steel and its exit tube is used as one of the electrodes forming ion
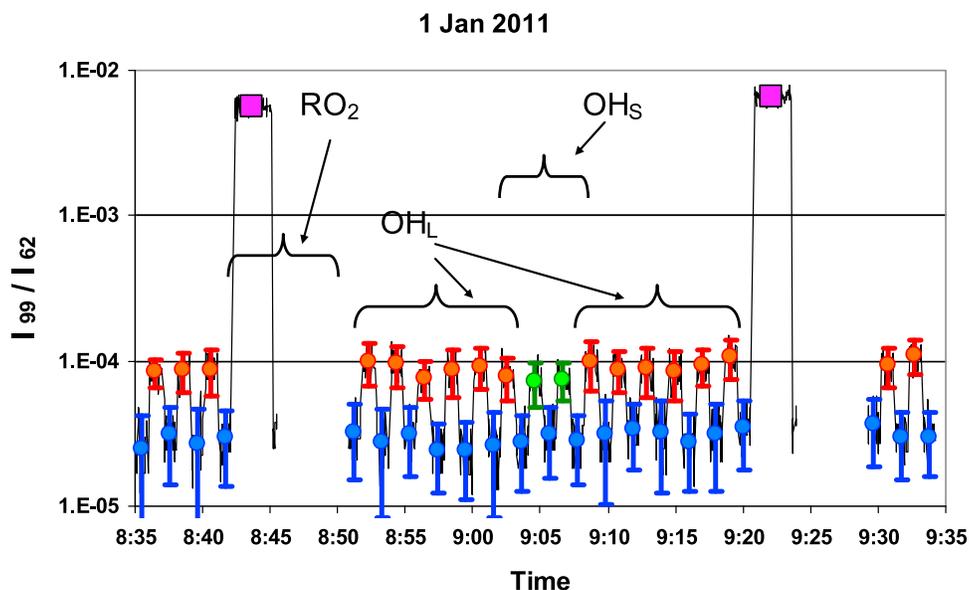
1 Jan 2011

Figure 2. Typical OH and RO$_2$ measurements sequence: blue, red, green and magenta points correspond to background, OH "long," OH "short" and RO$_2$ signals, respectively. The vertical error bars correspond to 1σ random deviation (see section 2.2).

trajectories in an ion-molecule reactor. The ion-molecule reactor has been also modified to allow addition of a "sheath" flow [*Tanner et al.*, 1997] resulted in a significant reduction of the background signal.

[15] Ambient air was sampled at a flow rate of 13 L min^{-1} creating turbulent flow conditions in the reactor to minimize possible wind speed influence and ensure fast mixing of reactants. The reactants used for chemical conversion (^{34}SO$_2$ and NO) and radical quencher (NO$_2$) are injected into the reactor through a set of injectors. Switching the reactant flows between the different injectors allows measurements in four different modes: a background mode, two different OH radical measurement modes and a RO$_2$ radical measurement mode. The two OH measurement modes differ by the time used for the chemical conversion, 3 and 20 ms. The short conversion time is usually employed for measurements in polluted environments to reduce the effect of artificial OH formation in the reaction of the HO$_2$ with ambient NO. In addition, ratio of the signals with the short and the long conversion times may be used as an indicator of an artificial OH formation in the reactor [*Kukui et al.*, 2008] and during the measurements at DDU both the long and the short modes were employed.

[16] OH, RO$_2$ and H$_2$SO$_4$ measurements were performed by monitoring the peak intensities at m/z = 62 (NO$_3^-$), m/z = 99 (H^{34}SO$_4^-$) and m/z = 97 (H^{32}SO$_4^-$). The detection of H^{34}SO$_4^-$ and H^{32}SO$_4^-$ corresponds to measurement of OH and H$_2$SO$_4$, respectively. A typical measurement sequence over one hour is shown in Figure 2. One minute measurements for each OH or background detection mode consisted of 25 samples of 1 s at m/z = 99 (OH) and 25 samples of 1s at m/z = 97 (H$_2$SO$_4$). Every 2 min OH measurement point included 1 min OH signal and two 30 s background signals on both sides of the OH signal. Typically several "short mode" and "long mode" OH points were measured in one sequence: 6 longs – 2 shorts – 6 longs in Figure 2. At the end of the OH measurement sequence NO was switched to the corresponding injector for the measurement of RO$_2$, typically for 2 min. To avoid any possible influence of traces of NO on the OH measurements the time delay of 10 min has been used before starting the next OH measurement sequence. For several periods the RO$_2$ measurements were interrupted and the OH measurements were performed without addition of NO into the reactor. No difference could be detected for the OH detection with NO or without it.

[17] Using data presented in Figure 2 that correspond to an OH concentration of (2.1 $\pm$ 0.3) $\times$ 10^6 molecule cm^{-3} (average value for the 30 min period from 8:50 to 9:20), we calculated a lower limit of detection of 8 $\times$ 10^5 molecule cm^{-3} for one 2 min OH point at signal-to-noise ratio of 3. Typical precision of the OH and RO$_2$ 15 min averaged data corresponding to a standard random deviation was better than $\pm$15% for OH concentrations higher than 10^6 molecule cm^{-3} and better than $\pm$5% for RO$_2$ levels higher than 10^8 molecule cm^{-3}.

2.3. Radical Measurement Calibration

[18] Calibration of the instrument was performed with a previously described calibration cell [*Kukui et al.*, 2008]. The calibration is based on production of controlled concentration of OH and RO$_2$ radicals in a turbulent flow reactor by photolysis of water vapor at 184.9 nm [*Heard and Pilling*, 2003, and references therein; *Faloona et al.*, 2004; *Dusanter et al.*, 2008]. The concentration of the radicals generated in the turbulent flow is calculated from the monitored photon flux and measured humidity. The ion peak intensities detected at m/z = 62 (I$_{62}$) and m/z = 99 (I$_{99}$) corresponding to the NO$_3^-$ and H^{34}SO$_4^-$ ions are related to the concentrations of radicals R (R = OH or HO$_2$) produced in a calibration unit by the following equation:

$$[R] = C_R \times \ln(1 + I_{97}/I_{62}).$$

[19] The calibration coefficients C_R can be derived from the estimated concentrations of radicals produced in the flow tube, [R], and the measured I_{97}/I_{62} ratio.

[20] The overall accuracy of the calibration coefficients is estimated taking into account uncertainties of all parameters used for calculation of the radical concentrations and the precision of the I_{97}/I_{62} measurements [Kukui et al., 2008]. The main source of the calibration uncertainty comes from the accuracy of estimation of the photon flux inside the reactor depending in particular on the uncertainty of photo-tube sensitivity. After the DDU campaign the calibration cell was retested by direct laboratory measurements of the OH concentrations produced in the cell. The calibration unit has been directly connected to a chemical ionization mass spectrometer, and OH concentrations were monitored by using ion molecule reaction with SF_6^- [Kukui et al., 2003]. In addition, somewhat different approach has been used in which OH was converted to HNO_3 by addition of NO_2 at sufficiently high concentrations. These experiments were performed in the absence of oxygen and H atoms produced by photolysis of H_2O were also converted to HNO_3 after their conversion to OH in the reaction with NO_2. HNO_3 was detected using the ion-molecule reaction with SF_6^-. The second method provided higher accuracy because the sensitivity to HNO_3 was higher and its concentration was two times higher than OH. Flow conditions and optical arrangement were unchanged with respect to that used at DDU. H_2O concentration in these experiments was higher than used at DDU, but according to calibration measurements the OH calibration coefficient does not depend on H_2O concentration. The calibration coefficient found in these experiments was 30% lower than used before and we used it for calculation of the radical concentrations presented in this work. For the new calibration coefficient the uncertainty (2σ) has been estimated to be of 25% for OH and of 30% for HO_2.

[21] The calibration of HO_2 and CH_3O_2 was performed by adding into the calibration cell photolysis reactor CO or CH_4 converting OH to HO_2 or CH_3O_2, respectively [Hanke et al., 2002; Fuchs et al., 2008]. The HO_2 calibration coefficient was always found to be 15% higher than that for the CH_3O_2. Under conditions of DDU the HO_2 and CH_3O_2 radicals represent the major part of the total peroxy RO_2 radicals with approximately equal contribution (see below). Consequently, the total peroxy concentration was calculated with the calibration coefficient average between HO_2 and CH_3O_2. The calibration uncertainty (2σ) for the RO_2 measurements accounting for possible variation of the RO_2 composition is estimated to be 35% under DDU conditions. Accounting for the calibration uncertainties and measurement precision, the overall 2σ uncertainty of the 15 min averaged measurements of OH and RO_2 is estimated to be 30% and 36%, respectively.

[22] Special caution was taken during the measurements at DDU to avoid a possible contamination of ambient air by NO and NO_2 reactants added to the chemical conversion reactor, especially, because first measurements revealed surprisingly high levels of radicals (see below). SO_2, NO and NO_2 injected into the reactor were trapped at pumps exhaust by using two 100 L cylinders containing zeolites. NO and NO_2 levels at the trap exit were found to be lower than 20 pptv (detection limit of the used NO_x monitor) for the freshly refilled cylinders. These cylinders were refilled

two times during measurements at DDU. Finally an exhaust tube of 30 m length was always placed downwind (prevailing direction) from the container. In numerous experiments when the exhaust tube was intentionally placed upwind and close to the radicals sampling point or when occasionally the wind pushed the exhausts toward the sampling point, no effect on radical measurements was however noticed.

3. Data Discussions

3.1. Data Presentation

[23] The records of OH and RO_2 covering the two weeks of measurements performed at DDU are presented in Figure 3. No measurements were conducted 31 December 2010, 8–10 and 12 January 2011 in relation with maintenance of the device or bad weather conditions (snowy), respectively. On several days, RO_2 were not measured to check possible influence of the NO reactant on ambient OH measurements (see section 2).

[24] Basic meteorological conditions encountered during the measurements are detailed in Preunkert et al. (submitted manuscript, 2012) including the results from a trajectory/dispersion model FLEXPART used to characterize the type of sampled air masses (marine boundary layer versus continental Antarctic air). In brief, during the campaign wind direction was predominantly either from east (100°E) or northwest (300°E). Note that the "iono" site is more impacted by penguin emissions when wind comes from east, while in the northwest sector there were no penguin colonies. Conditions with wind coming from the sector where the main DDU station activities take place (wind direction ranging between 0 and 45°E; see Figure 3) were occasionally apparent disturbing the CO record (Preunkert et al., submitted manuscript, 2012). These sporadic events were accompanied by obvious disturbance of radical measurements, for example on 3, 6 and 11 January. The corresponding data were discarded when calculating averaged values. As seen in Figure 3, most of the time the measurements were performed in air masses of the continental origin. Significant marine inputs were rather rare, late afternoon of 2 January, each afternoon from 5 to 6 January, and during the 7 to 9 January snowstorm.

[25] Ranges and averages of RO_2 and OH concentrations are summarized in Table 2. Maximum OH and RO_2 concentrations reached around 6×10^6 and 6×10^8 molecule cm^{-3}, respectively, being the highest values observed in Antarctica (see Table 1). Noon time OH and RO_2 median concentrations were 3.3×10^6 and 5.1×10^8 molecule cm^{-3}, respectively. Detectable OH and RO_2 levels were observed at night being at largest solar zenith angles about 20 and 10 times lower than their corresponding mean noon values, respectively. Although radiation measurements were not reliable during the night, sunlight was still present possibly explaining the detectable level of radicals.

3.2. Relationship With Estimated Photolysis Rates

[26] Atmospheric concentrations of OH and peroxy radicals under sunlight conditions result from primary generation via different mostly photolytic processes, interconversion of OH and RO_2 in reactions involving various trace gas molecules, and loss of radicals. Involved mechanisms depend on atmospheric environments including variable contribution of
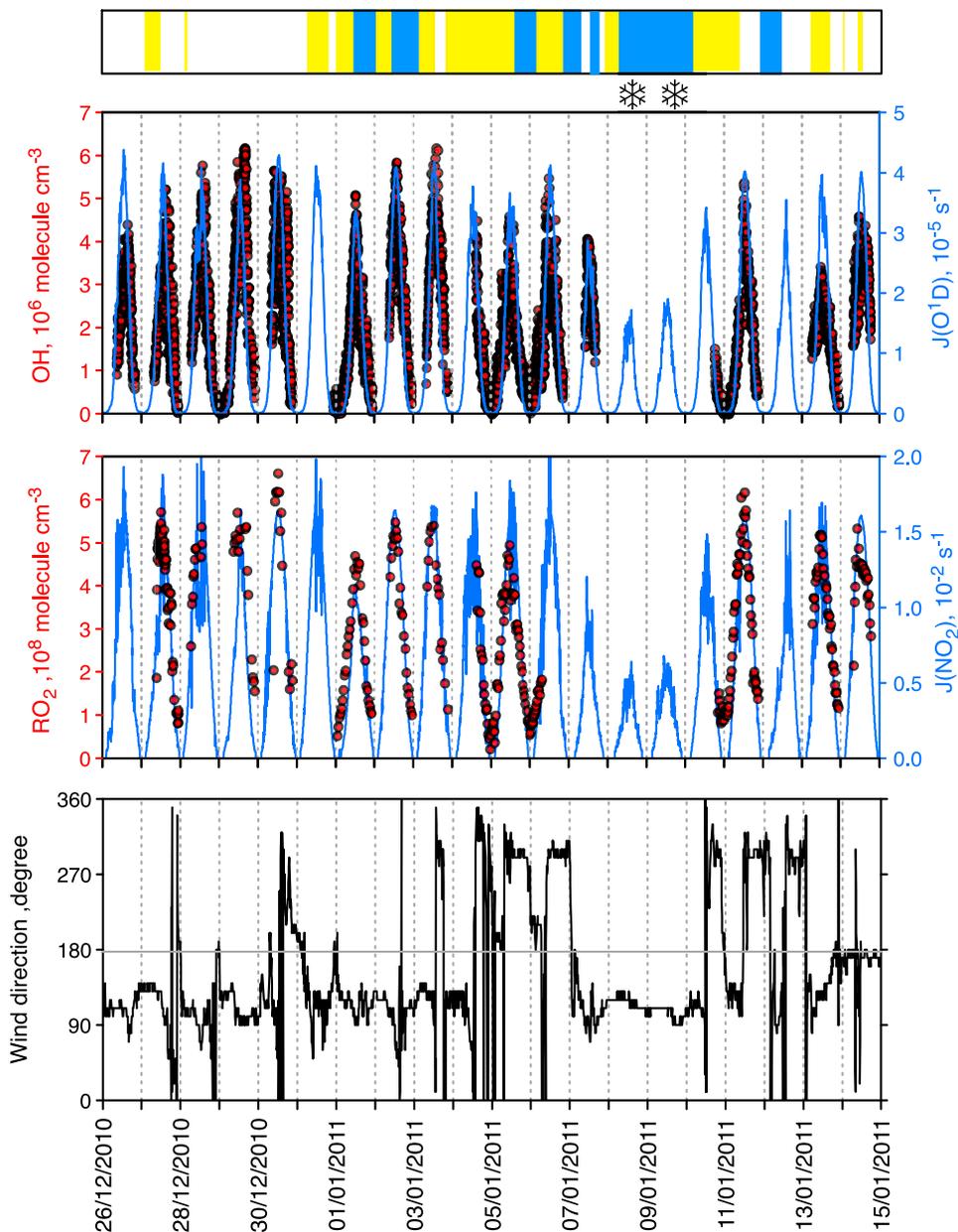
Figure 3. Observed (top) OH and (middle) RO$_2$ concentrations at DDU (dots) along with estimated O$_3$ and NO$_2$ photolysis rates (blue continuous lines). (bottom) Surface wind direction during measurements (0° corresponds to North). Yellow and blue bars at the top refer to time periods characterized by purely continental and mixed (marine and continental) conditions, respectively (see detail in Preunkert et al., submitted manuscript, 2012). Snowflakes show days when snow fall was observed.

Table 2. OH and RO$_2$ Concentrations Observed at DDU[a]

	Daily		Noon (11:00–14:00 Local Time)		Midnight (≈1:00 Local Time)	
	OH	RO$_2$	OH	RO$_2$	OH	RO$_2$
Range	<6.2 × 10^6	(0.2–6.6) × 10^8	(1.9–6.2) × 10^6	(4–6.6) × 10^8	(<LOD-8) × 10^5	(0.2–1) × 10^8
Median	2.0 × 10^6	3.6 × 10^8	3.3 × 10^6	5.1 × 10^8	2 × 10^5	6.7 × 10^7
Mean	2.1 × 10^6	3.3 × 10^8	3.6 × 10^6	5.0 × 10^8		

[a]Data are obtained directly from raw data (without 15 min averaging).

$$[OH]/10^5\,cm^{-3} = 9.5 \times J(O^1D)/10^{-5}s^{-1} \qquad + 7.5 \quad (R^2=0.68);$$
$$= 15.8 \times \left(J(O^1D)/10^{-5}s^{-1}\right)^{0.56} + 0.3 \quad (R^2=0.71);$$
$$= 21.0 \times J(NO_2)/10^{-2}s^{-1} \qquad + 2.8 \quad (R^2=0.72);$$
$$[RO_2]/10^7\,cm^{-3} = 26.0 \times J(NO_2)/10^{-2}s^{-1} \quad + 10.2 \quad (R^2=0.79);$$
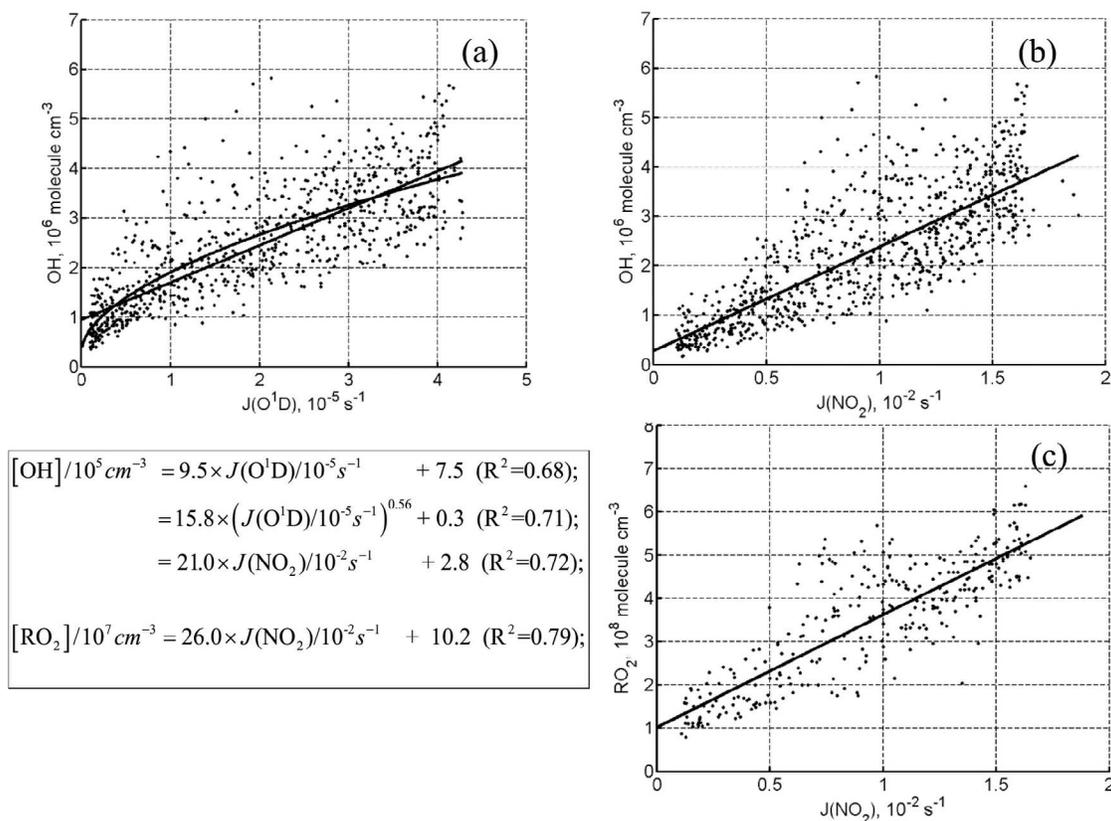
Figure 4. Dependences of OH on (a) J(O^{1}D) and (b) J(NO$_2$) and (c) of RO$_2$ on J(NO$_2$). Solid lines refer to linear and power dependencies weighted least square fits, respectively. The R^2 is the coefficient of multiple determination, calculated as the ratio of the sum of squares of the regression and the total sum of squares.

different photolytic sources (O$_3$, HCHO, HONO and others), and different composition and levels of trace gases participating in the radical interconversion and termination reactions (NO, NO$_2$, VOC, halogen species, etc.). Despite this diversity, the atmospheric steady state radical levels are usually found to follow solar radiation with close to linear correlation of the OH levels and J(O^{1}D), the rates of ozone photolysis [*Ehhalt and Rohrer*, 2000], representing usually significant OH production term. The dependence of OH on J(O^{1}D) is frequently described in more general form using an empirical power-low function [*Smith et al.*, 2006; *Rohrer and Berresheim*, 2006], [OH] = a × J(O^{1}D)^b + c, where the coefficients a, b and c derived from statistical analysis of OH and J(O^{1}D) measurements are considered to characterize a relation of the OH levels with a specific atmospheric chemical environment.

[27] As seen in Figure 3 the well-marked diurnal cycles of OH and RO$_2$ at DDU closely followed the estimated NO$_2$ and O$_3$ photolysis rates. The dependencies of OH on J(O^{1}D) and J(NO$_2$) and of RO$_2$ on J(NO$_2$) are presented in Figure 4. In order to quantify the correlation of OH and RO$_2$ with J(O^{1}D) and J(NO$_2$) the dependencies were described with both linear and power law fits with coefficients reported in Figure 4. For the correlation of OH and J(O^{1}D) both the linear and the exponential fits provide similar fitting goodness with R^2 of 0.68 and 0.71, respectively, indicating that the variation of solar UV radiation together with the variance

due to imprecision of the OH measurements (about 10%) explains about 80% of the total variance of OH.

[28] The slope of the linear fit of the OH on J(O^{1}D) dependence relates steady state OH level with solar UV radiation by incorporating a combined effect on OH of a specific chemical environment. The value of this slope at DDU was found to be 0.95 × 10^{11} molecule s cm^{-3} (or 1.2 × 10^{11} molecule s cm^{-3} if the intercept is fixed at 0). Slightly higher but similar slope values were obtained during some other campaigns in remote environments (1.7 × 10^{11} during the NUMBLEX campaign on the west coast of Ireland [*Smith et al.*, 2006]; 1.4 × 10^{11} during the ALBATROSS in Tropical Atlantic [*Brauers et al.*, 2001]). In comparison with the results of *Bloss et al.* [2007] during the CHABLIS campaign at Halley at the west coast of Antarctica the value of this coefficient is about 5 times higher under conditions of DDU. This difference, although its major part can be explained by higher at DDU levels of O$_3$ (on average about 3 times) and H$_2$O$_2$ (see Table 1), also indicates importance at DDU of some other than at Halley OH sources, like, for example, more efficient recycling from peroxy radicals.

[29] Although correlation coefficients of the linear and the power fits of the dependence of OH on J(O^{1}D) are only slightly different, visual inspection of the scatterplot shows that the power fits provide better description, while the intercept of the linear fit corresponds to a too high nighttime OH concentration, about 5 times higher than observed. The

exponent of the power dependence fit (0.56) is close to the exponent value of 0.53 found for the dependence of J(NO$_2$) on J(O^{1}D). Accordingly, there is a linear correlation of OH with J(NO$_2$). The value of exponent reflects a combined effect of all the photolytic processes producing OH directly or indirectly, e.g., via recycling from HO$_2$ [*Rohrer and Berresheim*, 2006]. Under conditions when production of OH is dominated by photolysis of ozone the dependence of OH on J(O^{1}D) is close to linear. The exponent of 0.56 indicates that OH levels at DDU were governed by a more complex mechanism, possibly including other than ozone species contributing to radical production, directly or via HO$_2$ recycling. Simple steady state analysis similar to that used by *Rohrer and Berresheim* [2006] shows that the dependence of OH on J(O^{1}D) becomes close to the power of 0.5 when, among other possible explanations, the recycling of HO$_2$ to OH becomes faster compared to OH production from photolysis sources and when the concentration of reactant participating in the conversion is only weakly dependent on photolysis rates. Interestingly, the same power dependence was found for the OH on J(O^{1}D) dependence obtained at Halley, although with a 5 times lower scaling coefficient, where a significant OH production pathway was the recycling of HO$_2$ to OH via reactions with halogen oxides [*Bloss et al.*, 2010]. Also, the same as at DDU exponent of 0.56 was found during the NUMBLEX campaign under conditions when NO levels were relatively high and consequently the contribution from HO$_2$ recycling to OH production was important [*Smith et al.*, 2006].

[30] The dependence of RO$_2$ on J(NO$_2$) observed at DDU is close to the linear (Figure 4c). Accounting for the typical quadratic dependence of J(O^{1}D) on J(NO$_2$), also found at DDU, this linear correlation suggests that O$_3$ photolysis is the main primary radical source and that self-reactions of peroxy radicals are the main radical loss pathway [*Penkett et al.*, 1997]. Overall, the observed at DDU correlations of OH and RO$_2$ with photolysis rates of O$_3$ and NO$_2$ are consistent with a mechanism in which the major total radicals loss is represented by self-reactions of peroxy radicals, the total radicals production is represented by photolytic processes linearly correlated with the photolysis of ozone and in which a conversion of HO$_2$ to OH represents a significant source of OH radicals.

3.3. Relationship With Air Mass Origin

[31] The correlation of OH and RO$_2$ with the photolysis rates together with imprecision of the measurements explains only 80% of the radical variability. To analyze the remaining sources of the radical variability the OH concentrations have been normalized to the square root of OH production rate from the photolysis of ozone, p(OH)$^{1/2}$. Indeed, linear dependency of OH on the square root of p(OH) is expected for NO$_x$ limited regime often observed in remote areas [*Jaeglé et al.*, 2001] and agrees with the dependencies of OH on the J(O1D) and J(NO$_2$) observed at DDU. Among available chemical measurements and local or regional meteorological data, the only meaningful correlation found with normalized radical levels was the one with the origin of sampled air masses derived from FLEXPART simulations (see section 3.1).

[32] According to this analysis, DDU was often under a strong influence of continental air masses except for a few occasions characterized by significant marine inputs (see section 3.1). An example of the arrival of an oceanic air mass at DDU is shown in Figure 5 for 5 January. The increase of transport from the ocean in the afternoon was accompanied by a significant decrease of normalized OH and RO$_2$ levels. Note that during that day wind was from south/southwest until 8:00 in the morning and from northwest for the rest of the day (Figure 3), two sectors virtually free of penguin colonies. The fast decrease of ozone and related increase of MSA in the afternoon is also a good indication that the change of oceanic fraction calculated by the transport model matches larger concentrations of species with well know oceanic sources and smaller ozone photochemical production. The increase of the ratio of CH$_3$OOH to the sum of H$_2$O$_2$ and CH$_3$OOH observed over the course of 5 January is also consistent with the enhanced contribution of marine air masses in which H$_2$O$_2$ is scavenged faster than CH$_3$OOH compared to conditions in a continental air mass [*Riedel et al.*, 2000].

[33] Considering all the OH data obtained during the campaign, the normalized OH concentrations are plotted against the oceanic contribution in Figure 6. Under conditions dominated by arrival of oceanic air masses at the site, the normalized OH level is about twice lower than the levels observed in purely continental air masses. The large scattering of the normalized OH values seen in continental air masses also indicates that the efficiency of the recycling mechanism can be very variable, depending for instance on the amount of NO or halogen oxides.

[34] Although halogen oxides were not measured at DDU, note that spatial and temporal variability of the tropospheric BrO columns show that regions with enhanced tropospheric BrO columns exhibit an excellent correlation with the areas of sea ice, located along the coast line of Antarctica [*Theys et al.*, 2011]. Therefore the bromine chemistry is thought to play a minor role at DDU, mostly because there is less sea ice in the Indian sector (DDU) than in the Atlantic sector (Halley) [*Legrand et al.*, 2009]. Year-round measurements of IO and BrO conducted at Halley by *Saiz-Lopez et al.* [2007] have shown that both species are present during the entire sunlit period and show similar seasonal cycles and concentrations. Though these similarities are not fully understood, it is likely that, as for BrO, the iodine chemistry would be less important at DDU than at Halley.

[35] The role of NO$_x$ chemistry in the recycling is more likely in continental air masses when there is a low dilution with local or oceanic sources considering the significant NO$_x$ mixing ratios (100–200 pptv) proposed by *Wang et al.* [2007] over the east flank of the Antarctic continent. The complex interaction between NO$_x$ and halogen chemistry remains possible for DDU, but a more thorough discussion about the respective effect of halogen and NO$_x$ is not possible in this study considering the lack of NO$_x$ and halogen measurements.

3.4. OH and RO$_2$ Sources and Sinks

[36] Sources and sinks of OH and RO$_2$ were estimated on the basis of relevant chemical measurements conducted at DDU during the OPALE campaign (see Table 1) and using relevant reaction rate coefficients from the MCM (version 3.2) photochemical box-model [*Jenkin et al.*, 1997;
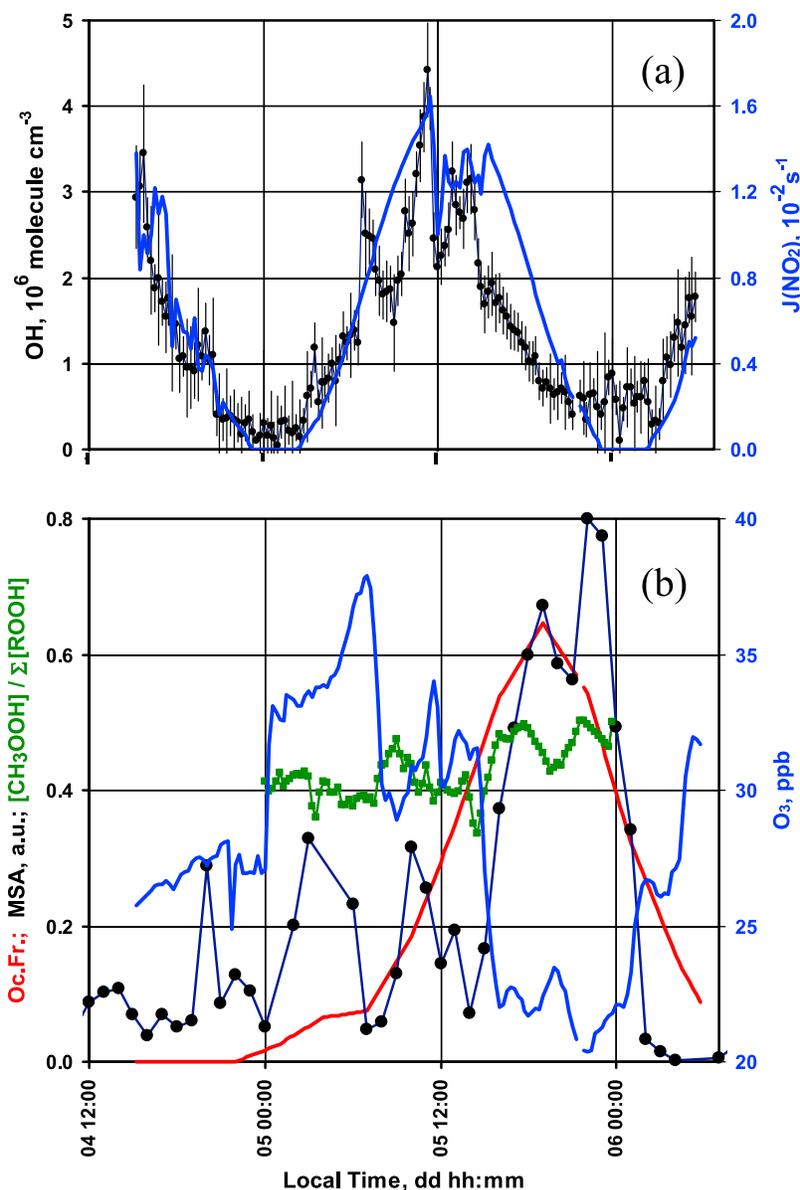
Figure 5. Influence of the changing air mass origins on the air chemistry from 4 to 6 January 2011. (a) Points refer to OH concentrations (with 1σ random deviations) and the blue curve is the estimated J(NO$_2$). (b) The red line refers to the oceanic fraction of air masses (denoted Oc.Fr.), black points to MSA levels, green points to the ratio of CH$_3$OOH to the sum of CH$_3$OOH and H$_2$O$_2$ (denoted Σ[ROOH]), and the blue line to the ozone mixing ratio (right scale).

Saunders et al., 2003]. The median diurnal changes of OH and RO$_2$ sources are shown in Figures 7 and 8.

[37] The primary OH production is largely dominated by the ozone photolysis followed by a 4 times lower contribution from the H$_2$O$_2$ photolysis. The contribution of the CH$_3$OOH photolysis is found to be less than 10% of the contribution from O$_3$ photolysis. For HONO, we have used the typical HONO mixing ratios of 2 pptv measured at DDU in February 2011 by *Kerbrat et al.* [2012]. The contribution of the HONO photolysis then becomes less than 20% of the O$_3$ photolysis contribution. Due to the high levels of acetaldehyde related to local penguin emissions, the loss of OH is dominated by the OH reaction with acetaldehyde (30%), exceeding the reactions with CO (29%) and methane (21%).

The contribution of other reactions including those involving O$_3$, H$_2$, HCHO and DMS remains in the range of 2–5%. The contribution of the reaction with NH$_3$ was very variable, with a mean value of 1%, but was sometimes as large as 10% when weather conditions favored ammonia production in ornithogenic soils (see details in *Legrand et al.* [2012]). The contribution from the reactions with acetic acid and acetone was less than 2%. The mean total reactivity of OH was 0.8 s^{-1}.

[38] The main primary source of peroxy radicals is the photolysis of HCHO with smaller contribution from the photolysis of acetaldehyde and methyl peroxide. The main process producing RO$_2$ is via the recycling reactions of OH with CH$_3$CHO, CO and CH$_4$. Note that RO$_2$ generation

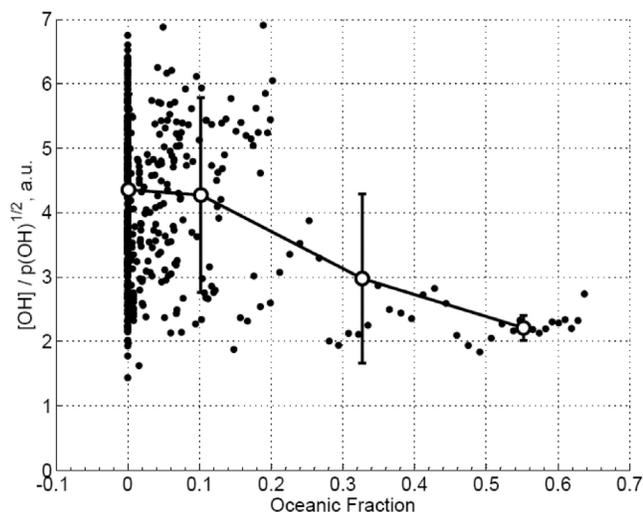**Figure 6.** Dependence of OH concentrations normalized to the square root of OH production rate from the photolysis of ozone (denoted p(OH)$^{1/2}$) on the origin of air masses (characterized by the Oceanic Fraction). Points refer to 15 min averaged data, circles to averages over different Oceanic fraction ranges (0, 0–0.2, 0.2–0.45, and 0.45–0.65).

via OH reactions was calculated using measured OH concentrations.

[39] The main RO$_2$ losses are the peroxy radical self-reactions. According to chemical data available at DDU, the peroxy radicals include HO$_2$, CH$_3$O$_2$ and CH$_3$COO$_2$ radicals. On the basis of steady state calculations made with the chemical mechanism from the MCM (version 3.2) [*Jenkin et al.*, 1997; *Saunders et al.*, 2003], the contribution of CH$_3$COO$_2$ radical produced by the OH oxidation of acetaldehyde is estimated to be less than 11%. As the chemical speciation of peroxy radicals depend on their inter-conversion rates, these HO$_2$, CH$_3$O$_2$ and CH$_3$OO$_2$ steady state calculations were done with several scenarios with respect to NO levels. The calculated contributions of HO$_2$, CH$_3$O$_2$ and CH$_3$OO$_2$ are, respectively, 29%, 60% and 11% in the absence of NO, 45%, 45% and 10% at 10 pptv of NO, 57%, 36% and 7% at 25 pptv of NO, and 69%, 26% and 5% at 50 pptv of NO. The RO$_2$ loss rate in the self-reactions of RO$_2$ (noon maximum of about 4×10^{-3} s^{-1}) depends weakly on the on the RO2 partitioning (<10%), when considering NO in the range of 0 to 50 pptv.

[40] Measured and calculated steady state concentrations of RO$_2$ and OH are compared in Figure 8. Two different steady state calculations were done. First, the concentration of the sum of OH and RO$_2$ was calculated without considering for any RO$_2$/OH inter-conversion reactions, but considering only for the primary OH and RO$_2$ radical sources. In a second approach, the steady state OH and RO$_2$ levels were estimated taking into account all OH and RO$_2$ sources and sinks including inter-conversion of RO$_2$ and OH. Although neither NO nor halogen oxides were measured at DDU, in order to estimate the importance of the recycling mechanisms, we performed steady state calculations assuming that HO$_2$ to OH and RO$_2$ inter-conversion processes were driven by reactions with NO.

[41] In the first approach, taking into account that OH are far less abundant than RO$_2$ and that the major loss of all, OH$^+$RO$_2$, radicals is the self-reaction of the peroxy radicals, the total peroxy radicals steady state concentrations are calculated from the following equation:

$$[RO_2] = (Sall/\Sigma k)^{1/2}$$

where Sall is the sum of radical production rates of all the primary photolysis processes, i.e., photolysis of O$_3$, HCHO, CH$_3$CHO, H$_2$O$_2$ and CH$_3$OOH, and Σk is the weighted sum
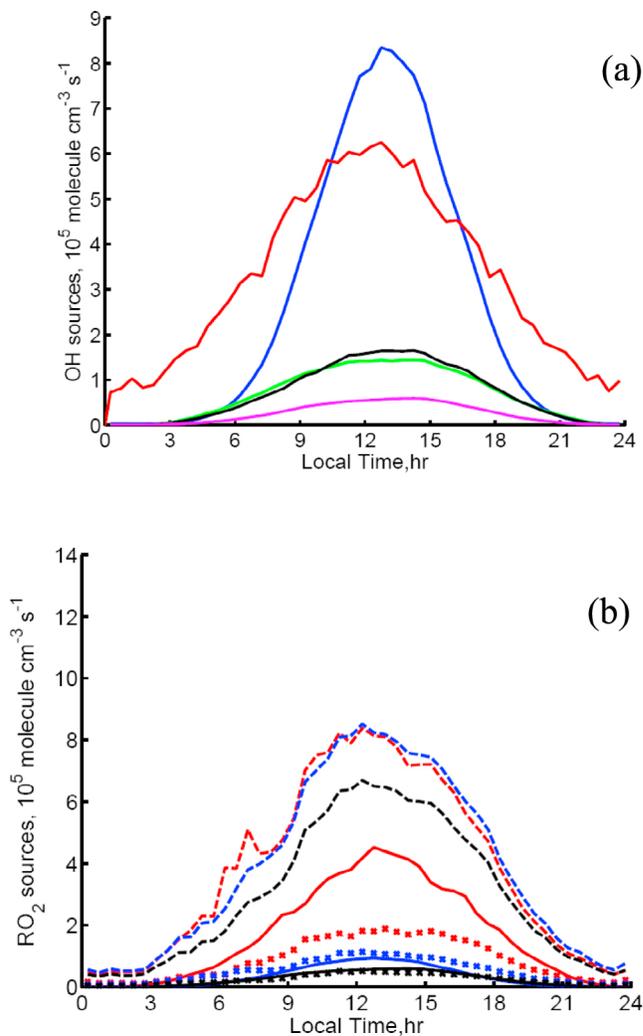

Figure 7. Mean diurnal profiles of production rates of (a) OH and (b) RO$_2$ radicals. In Figure 7a, blue line refers to O$_3$ photolysis, black line to HONO photolysis, green line to H$_2$O$_2$ photolysis, magenta line to CH$_3$OOH photolysis, and red line to the HO$_2$+NO reaction (assuming 10 pptv of NO). In Figure 7b, solid lines correspond to photolysis of HCHO (red), CH$_3$CHO (blue) and CH$_3$OOH (black). Dashed and dotted lines correspond to reactions of OH with CH$_3$CHO (dashed red), CO (dashed blue), CH$_4$ (dashed black), CH$_3$OOH (dotted red), O$_3$ (dotted blue), H$_2$O$_2$ (dotted black).
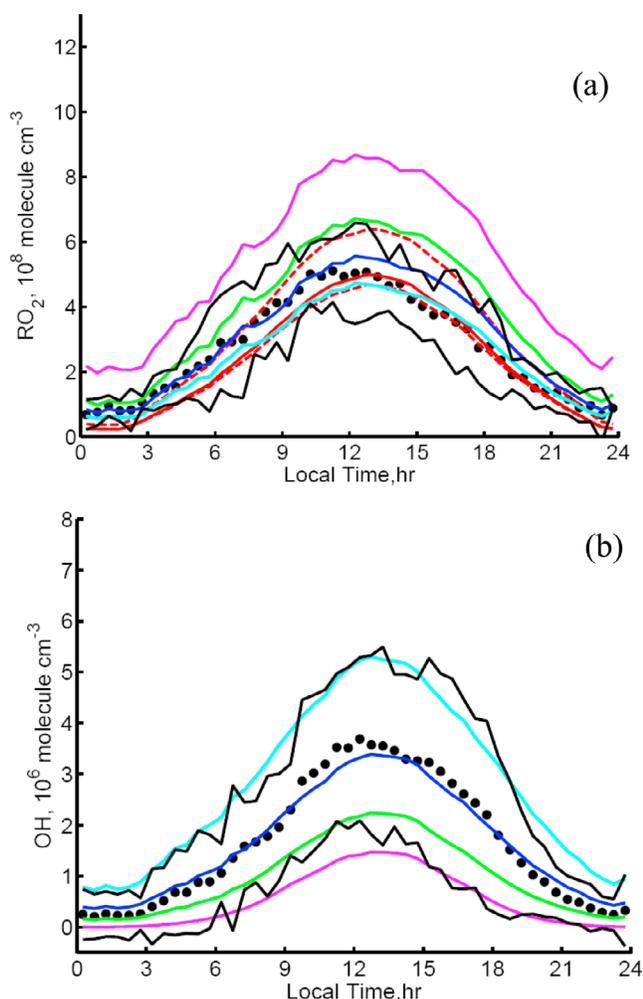
Figure 8. Comparison of measured and steady state calculated mean diurnal profiles of (a) RO$_2$ and (b) OH radicals. Black points and lines refer to means and 2σ standard deviations of observations, respectively. Magenta, green, blue, and cyan lines represent steady state calculations assuming NO levels of 0, 10, 25 and 50 pptv, respectively. The three red lines (one solid and two dashed) given in Figure 8a represent RO$_2$ steady state calculations for primary radical sources. The upper, middle, and lower lines correspond to the RO$_2$ composition assuming NO levels of 0, 25 and 50 pptv, respectively.

of the rate constants of the removing RO$_2$ self-reactions of HO$_2$, CH$_3$O$_2$ and CH$_3$COO$_2$ radicals. The assumption we made that the self-peroxy radicals reactions are the major radical removal pathway seems to be reasonable under the DDU conditions, since the removal of radicals from the reaction of OH with NO$_2$ would imply unrealistic NO$_2$ level of more than 1 ppbv. Also, this assumption is consistent with observed at DDU linear correlation of RO$_2$ with J(NO$_2$), as discussed above. As the term Σk depends on the RO$_2$ composition, the steady state diurnal profiles of RO$_2$ were calculated with 3 different HO$_2$, CH$_3$O$_2$ and CH$_3$OO$_2$ partitionings corresponding to inter-conversion mechanism with 0, 25 and 50 pptv of NO. The steady state RO$_2$ profiles calculated using this method are only slightly dependent on

the RO$_2$ composition and are in good agreement with measurements (red curves in Figure 8a), suggesting that available chemical records at DDU are sufficient to account for all significant radical sources and explain the observed levels of RO$_2$ radicals.

[42] In the second approach, the OH and RO$_2$ steady state diurnal profiles were calculated using the measured RO$_2$ and OH concentrations, respectively, to account for the radical recycling in addition to the primary sources. The results of these calculations at different NO mixing ratios are presented in Figure 8a for RO$_2$ and in Figure 8b for OH. As can be seen, the steady state OH and RO$_2$ profiles without accounting for a possible RO$_2$ to OH conversion significantly overestimate the RO$_2$ and underestimate OH concentrations, indicating that some RO$_2$ to OH conversion mechanism is missed. The calculated median profiles are in very good agreement with measurements for the RO$_2$ to OH conversion equivalent to a mean NO mixing ratio of 25 pptv. When considering variability of the diurnal cycle of OH and RO$_2$ (solid black lines in Figures 8a and 8b corresponding to 2σ deviation), the radical measurements can be described with NO levels ranging from 10 to 50 pptv. The same results could be obtained using for the OH steady state calculation the RO$_2$ levels derived from the steady state calculations of the first type accounting only for the primary radical sources which are in good agreement with the measured RO$_2$. Note also that the conclusion about importance of the radical inter-conversion at DDU is consistent with the results derived from the presented above discussion of the dependence of OH on J(O^{1}D).

4. Discussion

4.1. Comparison With Other Studies in Coastal Antarctica

[43] The OH concentrations at DDU are about 4–5 times higher than those observed at other coastal Antarctic sites of Halley [*Bloss et al.*, 2010] and Palmer [*Jefferson et al.*, 1998]. At the same time, the RO$_2$ concentrations are about 10 times higher at DDU than HO$_2$ measured at Halley.

[44] Although measurements at DDU are less complete than at Halley they also support the conclusion that the photolysis of O$_3$ and HCHO represents the major source of radicals, accounting for about 80% of the radical production. The O$_3$ photolysis is however about 2.5 times faster at DDU than at Halley due to higher O$_3$ levels, while the production from HCHO is about 30% faster. Overall, the total radical production rate is about twice faster at DDU compared to Halley. As the RO$_2$ concentration is proportional to the square root of the radical production rate under conditions of main removal process driven by RO$_2$ self-reactions, the RO$_2$ at Halley would be only about 70% less than at DDU, in agreement with model simulations presented in *Bloss et al.* [2010]. At the same time, the measured HO$_2$ levels at Halley are about 3–4 times lower compared to both the model prediction and to the HO$_2$ at DDU that can be roughly estimated as a half of measured total RO$_2$ (see section 3.4). The reason for this difference in the measured peroxy radical levels under conditions of similar rates of radical production as well as for the discrepancy of the measured and the modeled concentrations at Halley is not clear.

[45] OH concentrations at DDU are significantly higher compared to the steady state estimations made by neglecting OH recycling mechanisms. When assuming a rate of recycling equivalent to about 25 pptv of NO needed to explain both the OH and RO$_2$ measurements at DDU, the low OH levels at Palmer are consistent with a lower influence of HO$_2$ to OH conversion at that site [*Jefferson et al.*, 1998]. Indeed very low NO concentrations were measured at Palmer. The lower OH levels observed at Halley compared to the OH levels found at DDU cannot be explained by a weaker HO$_2$ to OH recycling at Halley considering the important role of the reactions of HO$_2$ with NO, BrO and IO observed for this site. The difference between model and measured OH concentrations at Halley suggests again a complex mechanism to account for the recycling of OH when there is a dominant role of halogen chemistry [*Bloss et al.*, 2010].

4.2. Representativeness of the DDU Site

[46] Due to the presence of large penguin colonies the concentration of some key species at DDU could be influenced by local emissions leading to a difference in the radical levels observed at DDU and at "background" conditions. As discussed by *Legrand et al.* [2012] the local emissions strongly affect the levels of ammonia, acetic acid, acetaldehyde, and acetone. The impact on HCHO is far less important and as described in *Pépy* [2011] it was noticeable only under low wind speed conditions. Derived from the DDU observations by interpolating the data filtered at the wind speed higher than 4 m s^{-1}, the "background" HCHO mixing ratio of 150 pptv are close to the measured at DDU concentrations of 160 pptv.

[47] Concentrations of the acetic acid, acetaldehyde, acetone and ammonia were significantly higher at DDU compared to the "background" levels of 100 pptv, 80 pptv, 130 pptv and 0 pptv, respectively [*Legrand et al.*, 2012]. However, the acetic acid, acetone and ammonia do not significantly affect the radical levels accounting only for less than 2% of the OH sinks. At the same time, the impact of the local emissions on the acetaldehyde being under the DDU conditions the major recycler of OH to RO$_2$ and the photolytic source of RO$_2$ may significantly influence the radical concentrations. From the comparison of calculated steady state concentrations of OH and RO$_2$ for the acetaldehyde levels measured at DDU and for the "background" level of 80 pptv we estimate that the local acetaldehyde emissions result in about 25% reduction and 10% increasing of the OH and RO$_2$ concentration levels, respectively.

[48] Finally, ornithogenic soils may release nitrogen species that are more oxygenated than ammonia, e.g., HONO, NO, and N$_2$O. The HONO photolysis represents a primary source of OH but, as discussed in *Legrand et al.* [2012], the well-marked alkalinity of ornithogenic soils at DDU strongly disfavors the release of this species. The insignificance of the HONO release from soils at that site was confirmed by HONO measurements made by *Kerbrat et al.* [2012]. To our knowledge no data on the release of NO from ornithogenic soils are available in the literature. To date, *Zhu et al.* [2008] reported a mean nitrous oxide of 850 μg N$_2$O-N m^{-2} h^{-1} in a penguin colony in the Antarctic Peninsula. Since the pH of soils at that site was close or below 5 [*Zhu et al.*, 2009], it is however difficult to extrapolate this value for the DDU site. Indeed, at such pH values

most of the mineralized nitrogen material will stay in the form of ammonium and nitrification of ammonium into more oxidized nitrogen species can go on, whereas at higher pH encountered at DDU, most of produced ammonium would escape to the atmosphere limiting the subsequent nitrification toward N$_2$O and NO.

5. Conclusions

[49] The OH and RO$_2$ concentrations observed at DDU from December 2010 to January 2011 are the highest ever measured in coastal Antarctica. Up to 15 diurnal cycles were recorded corresponding to different transport regimes, mainly from inland Antarctica, but also two clear marine cases. The 2σ uncertainty of the radical measurements is 30% for OH and 36% for RO$_2$, accounting for the calibration uncertainty and measurements precision. Although photolysis coefficients were not directly measured, they could be derived from other photometric measurements with 20%–30% accuracy. An analysis of the diurnal cycle of peroxy radicals was performed using steady state calculation of RO$_2$ with concurrent measurements made at the site. There is a very good agreement between the RO$_2$ observations and the steady state calculations showing also a dominant role of O$_3$ and HCHO photolysis. However, the observed OH level of 2 $\times$ 10^6 molecule cm^{-3} could not be explained without assumption about significant contribution of RO$_2$ recycling to the production of OH. For instance, the 24 h average OH level at DDU would be about 7 $\times$ 10^5 molecule cm^{-3} when accounting only for the primary OH sources. The steady state concentration analysis implies a RO$_2$ to OH conversion mechanism equivalent to the presence of NO in the range from 10 to 50 pptv to explain observed OH and RO$_2$ concentrations. The conversion with some 25 pptv of NO explains the OH and RO$_2$ mean diurnal profiles. As neither NO nor halogen oxides were measured at DDU, the mechanism of this recycling could not be explicitly identified. However, the analysis of the origin of sampled air masses shows that the OH recycling would be more efficient in continental air masses. First, the comparison of radical measurements in marine and continental air masses normalized to OH primary production, second, the absence of sea ice in the Indian sector (DDU) compared to the Atlantic sector (Halley) suggest a weaker influence of halogen chemistry at DDU than in West Antarctica. Without either NO or halogen oxides measurements it is not possible to further discuss mechanism of the RO$_2$/OH inter-conversion. Additional studies including the measurements of NO$_x$, photolysis rates and, possibly, halogen compounds are certainly needed to constrain better the analyses of the present observations.

Appendix A: Estimation of Photolysis Rates

[50] Knowledge of photolysis rates is important when discussing the radical data. Unfortunately, no direct actinic flux measurements are available for the DDU OPALE campaign. Therefore, they have been estimated using global erythemal irradiance and total global irradiance routinely measured at DDU, together with the Tropospheric Ultraviolet and Visible radiation (TUV) model, version 5.0. [*Madronich*, 1993] using the 8-stream discrete ordinate
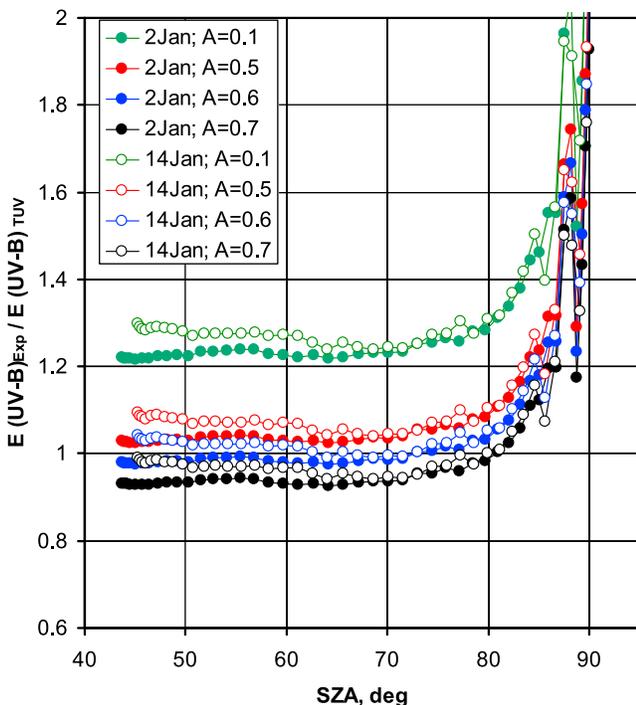
Figure A1. Ratio between measured and calculated global erythemal irradiance as a function of the solar zenith angle (SZA) for different single-scattering surface albedo values. The colors black, blue, red and green refer to albedo values of 0.7, 0.6, 0.5, and 0.1 respectively. Closed and open circles represent data from 2 and 14 January, respectively.

method with a pseudo-spherical correction [*Dahlback and Stamnes*, 1991].

[51] A UV broadband radiometer (Solar Light UV Biometer model 501) is used at DDU for continuous measurements of the 5 min averaged erythemally weighted UV-B global irradiance in the wavelength range of 280–320 nm. The spectral response of the Biometer is close to the CIE (Commission Internationale de l'Eclairage) standard human erythemal action spectrum [*McKinlay and Diffey*, 1987] and it is calibrated to show the biological effectiveness of the solar radiation according to the CIE standard. The radiometer was installed on the roof of a building on the altitude of about 40m above the ocean and had 2π field of view with uninterrupted flat horizon. Biometer data are corrected for the ozone column density [*Pommereau and Goutail*, 1988] and cosine error using tabulated correction functions determined during the last instrument calibration. The total downwelling solar irradiance in spectral range 335–2800 nm is continuously monitored at DDU with a Kipp and Zonen 6B Pyranometer.

[52] The O$_3$ photolysis rates, J(O^{1}D)^{est}, are estimated from the measured CIE UV-B irradiance, E$_{CIE}^{exp}$ since the UV broadband radiometer measures a weighted irradiance in the key wavelength region for the photolysis of ozone in the troposphere:

$$J\left(O^1D\right)^{est} = R^{mod} \times E_{CIE}^{exp}, \qquad (A1)$$

where R^{mod} is the ratio of the (TUV) model-calculated O$_3$ photolysis rate to the (TUV) model-calculated CIE irradiance. In general, R^{mod} is a function of zenith angle, surface albedo and atmospheric parameters, including those related to effects of clouds and aerosols.

[53] The UV-B calculations are performed over the 120–730 nm wavelength range divided in 158 intervals using the default TUV grid. A number of input parameters to the model are regularly measured at DDU such as the ozone column density and meteorological parameters (pressure and temperature). Background aerosols in coastal Antarctica are typically composed of weak absorbing sea salt and sulphate aerosols and do not significantly affect the UV and visible solar radiation [*Chaubey et al.*, 2011, and references therein]. For all calculations, the aerosol optical depth is set to 0.035 [*Chaubey et al.*, 2011]. The most important parameters for the model-calculated irradiances and actinic fluxes are surface albedo and the cloud properties.

[54] The surface albedo is estimated by matching model-calculated and measured CIE irradiances for the clear sky (cloud-free) conditions encountered on the days of 2 January and 14 January of 2011. The ratio of the model-calculated to the measured CIE irradiance for the 2 and 14 January is plotted as a function of the solar zenith angle, SZA, in Figure A1 for different values of albedo. For both days, corresponding approximately to the beginning and the end of the measurements campaign, an albedo of about 0.6 provides the best agreement between the measured and calculated CIE irradiances. The reasons for the deviation of the ratio at large SZA (SZA > 80) are not clear. It could be attributed to measurements errors at large SZA.

[55] Our albedo value of 0.6 derived from clear sky erythemal irradiance is lower than the values of about 0.9 usually observed at Antarctica in-land sites covered with snow [*Bernhard et al.*, 2005]. However, at coastal sites, the presence of the open ocean (with a surface albedo of about 0.05) and snowmelting result in a lower albedo. For example, at Palmer station, this leads to an albedo varying from 0.8 in winter to 0.4 in summer [*Bernhard et al.*, 2005]. According to simulations by *Mayer and Degünther* [2000], the regional albedo at DDU should be around 0.5 in summer. The slightly higher albedo derived here from the erythemal irradiance can be related to an effective albedo of the ocean surface which was higher because the ocean was not completely ice free, but frequently with icebergs and drift ice blown in. In our study a constant albedo of 0.6 is used for all calculations, assuming an error of ±0.1.

[56] The impact of clouds on R^{mod} of equation (A1) is considered by investigating R^{mod} for a surface albedo of 0.6 and cloud optical depths ranging from 0 to 100. The calculations were performed for a clouds base and a clouds height of 1 km and 2 km, respectively, most frequently observed for the low level clouds over DDU [*Del Guasta et al.*, 1993]. The variations of R^{mod} are smaller than 5% for COD varying from 5 to 100, what is not surprising since clouds are expected to have a somewhat similar effect on J(O1D) and UV-B radiation.

[57] The dependencies of R^{mod} on SZA at COD = 0 and COD > 5 for an albedo of 0.6 are approximated with polynomial functions of the SZA, and then used for the calculation of the J(O^{1}D) in equation (A1). In doing so, the

polynomial function of COD = 0 is used for the two clear sky days and the one corresponding to COD > 5 for all the other days, respectively.

[58] The same approach as for the photolysis rate of ozone is used for the estimation of the NO$_2$ photolysis rates, J(NO$_2$). Because the photolysis of NO$_2$ is dominated by visible radiation, J(NO$_2$) are estimated from the measured total irradiances, E$_{tot}$ using a relationship of the type of equation (A1) with a function R^{mod} derived from the model calculations of J(NO$_2$) and modeled total irradiance. The albedo was assumed to be the same as for the UV calculations. Since, the TUV model covers only the 300 to 1000 nm wavelength region whereas the total irradiance is measured in the 335 to 2800 nm range, the ratio between modeled and measured total irradiance was checked for its stability versus SZA variations during the two clear sky days of our campaign. The ratios estimated for both days are found to be in excellent agreement and in addition more or less independent of SZA for angles <75°. As observed for J(O^{1}D), R^{mod} of J(NO$_2$) varies very little with COD ranging from 0 to 100 for an albedo of 0.6 In addition R^{mod} of J(NO$_2$) varies with SZA by less than 5% for angles <75°.

[59] Estimated J(NO$_2$) and J(O^{1}D) are presented in Figure 3 for the period of the measurements campaign at DDU. The photolysis rates of other species, important for photochemical modeling, are approximated by fitting the model-calculated photolysis rates with a quadratic function of the model-calculated J(O^{1}D) and J(NO$_2$) for an albedo of 0.6 and COD varying from 0 to 100. This parameterization is similar to the parameterization used by *Holland et al.* [2003].

[60] The overall uncertainty of the derived O^{1}D) and J(NO$_2$) values was estimated for the solar zenith angle smaller than 75° accounting for sensitivity of the R^{mod} function (equation (A1)) to the uncertainty of the used albedo value, goodness of the fits used to describe the ratio of the calculated photolysis rates to the calculated CIE or the total irradiances, for J(O^{1}D) and J(NO$_2$), respectively, and the uncertainty of the measured CIE and total irradiance measurements. The estimated uncertainty of the albedo value, 0.6 ± 0.1, results in 10% uncertainty of R^{mod}. The deviation of the calculated J(O^{1}D)/E$_{CIE}$ and J(NO$_2$)/E$_{Tot}$ from the polynomial fit is less than 5%. Based on the technical specification given by manufactures, the 1σ uncertainties of the CIE and total irradiance measurements are estimated to be of 10% and of 15%, respectively. Combining these uncertainties we estimate for SZA < 75° uncertainties of 20% and 25% for J(O^{1}D) and J(NO$_2$), respectively. The uncertainty for the photolysis rates of other species used in this work, HONO, HCHO, CH$_3$CHO, H$_2$O$_2$ and CH$_3$OOH, are estimated to be of 30%.

References

Bernhard, G., C. R. Booth, and J. C. Ehramjian (2005), UV climatology at Palmer Station, Antarctica, based on Version 2 NSF network data, in *Ultraviolet Ground- and Space-Based Measurements, Models, and Effects V*, edited by G. Bernhard et al., *Proc. SPIE Int. Soc. Opt. Eng.*, *5886*, 1–12.

Berresheim, H., T. Elste, C. Plass-Dülmer, F. L. Eiseleb, and D. J. Tanner (2000), Chemical ionization mass spectrometer for long-term measurements of atmospheric OH and H$_2$SO$_4$, *Int. J. Mass Spectrom.*, *202*, 91–109, doi:10.1016/S1387-3806(00)00233-5.

Bloss, W. J., J. D. Lee, D. E. Heard, R. A. Salmon, S. J.-B. Bauguitte, H. K. Rosco, and A. E. Jones (2007), Observations of OH and HO$_2$ radicals in coastal Antarctica, *Atmos. Chem. Phys.*, *7*, 4171–4185, doi:10.5194/acp-7-4171-2007.

Bloss, W. J., M. Camredon, J. D. Lee, D. E. Heard, J. M. C. Plane, A. Saiz-Lopez, S. J.-B. Bauguitte, R. A. Salmon, and A. E. Jones (2010), Coupling of HO$_x$, NO$_x$ and halogen chemistry in the Antarctic boundary layer, *Atmos. Chem. Phys.*, *10*, 10,187–10,209, doi:10.5194/acp-10-10187-2010.

Brauers, T., M. Hausmann, A. Bister, A. Kraus, and H. P. Dorn (2001), OH radicals in the boundary layer of the Atlantic Ocean: 1. Measurements by long-path laser absorption spectroscopy, *J. Geophys. Res.*, *106*(D7), 7399–7414, doi:10.1029/2000JD900679.

Chaubey, J. P., K. K. Moorthy, S. S. Babu, and V. S. Nair (2011), The optical and physical properties of atmospheric aerosols over the Indian Antarctic stations during southern hemispheric summer of the International Polar Year 2007–2008, *Ann. Geophys.*, *29*, 109–121, doi:10.5194/angeo-29-109-2011.

Chen, G., et al. (2007), An assessment of the polar HO$_x$ photo-chemical budget based on 2003 Summit Greenland field observations, *Atmos. Environ.*, *41*, 7806–7820, doi:10.1016/j.atmosenv.2007.06.014.

Dahlback, A., and K. Stamnes (1991), A new spherical model for computing the radiation field available for photolysis and heating at twilight, *Planet. Space Sci.*, *39*(5), 671–683, doi:10.1016/0032-0633(91)90061-E.

Davis, D., et al. (2001), Unexpected high levels of NO observed at South Pole, *Geophys. Res. Lett.*, *28*, 3625–3628, doi:10.1029/2000GL012584.

Del Guasta, M., M. Morandi, M. Stefanutti, J. Brechet, and J. Piquad (1993), One year of cloud lidar data from Dumont d'Urville (Antarctica): 1. General overview of geometrical and optical properties, *J. Geophys. Res.*, *98*(D10), 18,575–18,587, doi:10.1029/93JD01476.

Dusanter, S., D. Vimal, and P. S. Stevens (2008), Technical note: Measuring tropospheric OH and HO$_2$ by laser-induced fluorescence at low pressure: A comparison of calibration techniques, *Atmos. Chem. Phys.*, *8*, 321–340, doi:10.5194/acp-8-321-2008.

Ehhalt, D. H., and F. Rohrer (2000), Dependence of the OH concentration on solar UV, *J. Geophys. Res.*, *105*, 3565–3571, doi:10.1029/1999JD901070.

Eisele, F. L., and D. J. Tanner (1991), Ion-assisted tropospheric OH measurements, *J. Geophys. Res.*, *96*(D5), 9295–9308, doi:10.1029/91JD00198.

Faloona, I. C., et al. (2004), A Laser-induced fluorescence instrument for detecting tropospheric OH and HO$_2$: Characteristics and calibration, *J. Atmos. Chem.*, *47*, 139–167, doi:10.1023/B:JOCH.0000021036.53185.0e.

Fuchs, H., F. Holland, and A. Hofzumahaus (2008), Measurement of tropospheric RO$_2$ and HO$_2$ radicals by a laser-induced fluorescence instrument, *Rev. Sci. Instrum.*, *79*, 084104, doi:10.1063/1.2968712.

Hanke, M., J. Uecker, T. Reiner, and F. Arnold (2002), Atmospheric peroxy radicals: ROXMAS, a new mass-spectrometric methodology for speciated measurements of HO$_2$ and ΣRO$_2$ and first results, *Int. J. Mass Spectrom.*, *213*, 91–99, doi:10.1016/S1387-3806(01)00548-6.

Heard, D. E., and M. J. Pilling (2003), Measurement of OH and HO$_2$ in the troposphere, *Chem. Rev.*, *103*, 5163–5198, doi:10.1021/cr020522s.

Holland, F., A. Hofzumahaus, J. Schäfer, and A. Kraus (2003), Measurements of OH and HO$_2$ radical concentrations and photolysis frequencies during BERLIOZ, *J. Geophys. Res.*, *108*(D4), 8246, doi:10.1029/2001JD001393.

Honrath, R. E., M. C. Peterson, S. Guo, J. E. Dibb, P. B. Shepson, and B. Campbell (1999), Evidence of NO$_x$ production within or upon ice particles in the Greenland snowpack, *Geophys. Res. Lett.*, *26*, 695–698, doi:10.1029/1999GL900077.

Honrath, R. E., M. C. Peterson, M. P. Dziobak, J. E. Dibb, M. A. Arsenault, and S. A. Green (2000), Release of NO$_x$ from sunlight-irradiated midland snow, *Geophys. Res. Lett.*, *27*, 2237–2240, doi:10.1029/1999GL011286.

Jaeglé, L., D. J. Jacob, W. H. Brune, and P. O. Wennberg (2001), Chemistry of HO$_x$ radicals in the upper troposphere, *Atmos. Environ.*, *35*, 469–489, doi:10.1016/S1352-2310(00)00376-9.

Jefferson, A., D. J. Tanner, F. L. Eisele, D. D. Davis, G. Chen, J. Crawford, J. W. Huey, A. L. Torres, and H. Berresheim (1998), OH photochemistry

and methane sulfonic acid formation in the coastal Antarctic boundary layer, *J. Geophys. Res.*, *103*(D1), 1647–1656, doi:10.1029/97JD02376.

Jenkin, M. E., S. M. Saunders, and M. J. Pilling (1997), The tropospheric degradation of volatile organic compounds: A protocol for mechanism development, *Atmos. Environ.*, *81*, 31–104, doi:10.1016/S1352-2310(96)00105-7.

Jones, A. E., R. Weller, P. S. Anderson, H.-W. Jacobi, E. W. Wolff, O. Schrems, and H. Miller (2001), Measurements of NO$_x$ emissions from the Antarctic snowpack, *Geophys. Res. Lett.*, *28*, 1499–1502, doi:10.1029/2000GL011956.

Kerbrat, M., M. Legrand, S. Preunkert, H. Gallée, and J. Kleffmann (2012), Nitrous acid at Concordia (inland site) and Dumont d'Urville (coastal site), East Antarctica, *J. Geophys. Res.*, *117*, D08303, doi:10.1029/2011JD017149.

Kukui, A., D. Borissenko, G. Laverdet, and G. Le Bras (2003), Gas-phase reactions of OH radicals with dimethyl sulfoxide and methane sulfinic acid using turbulent flow reactor and chemical ionization mass spectrometry, *J. Phys. Chem. A*, *107*, 5732–5742, doi:10.1021/jp0276911.

Kukui, A., G. Ancellet, and G. Le Bras (2008), Chemical ionisation mass spectrometer for measurements of OH and Peroxy radical concentrations in moderately polluted atmospheres, *J. Atmos. Chem.*, *61*(2), 133–154, doi:10.1007/s10874-009-9130-9.

Legrand, M., F. Ducroz, D. Wagenbach, R. Mulvaney, and J. Hall (1998), Ammonium in coastal Antarctic aerosol and snow: Role of polar ocean and penguin emissions, *J. Geophys. Res.*, *103*, 11,043–11,056, doi:10.1029/97JD01976.

Legrand, M., S. Preunkert, B. Jourdain, H. Gallée, F. Goutail, R. Weller, and J. Savarino (2009), Year round record of surface ozone at coastal (Dumont d'Urville) and inland (Concordia) sites in East Antarctica, *J. Geophys. Res.*, *114*, D20306, doi:10.1029/2008JD011667.

Legrand, M., V. Gros, S. Preunkert, R. Sarda-Estève, A.-M. Thierry, G. Pépy, and B. Jourdain (2012), A reassessment of the budget of formic and acetic acids in the boundary layer at Dumont d'Urville (coastal Antarctica): The role of penguin emissions on the budget of several oxygenated volatile organic compounds, *J. Geophys. Res.*, *117*, D06308, doi:10.1029/2011JD017194.

Madronich, S. (1993), UV radiation in the natural and perturbed atmosphere, in *UV-B Radiation and Ozone Depletion. Effects on Humans, Animals, Plants, Microorganisms, and Materials*, edited by M. Tevini, pp. 17–69, Lewis, Boca Raton, Fla.

Mauldin, R. L., et al. (2001), Measurements of OH, H$_2$SO$_4$, and MSA at the South Pole during ISCAT, *Geophys. Res. Lett.*, *28*(19), 3629–3632, doi:10.1029/2000GL012711.

Mauldin, R. L., E. Kosciuch, B. Henry, F. L. Eisele, R. Shetter, B. Lefer, G. Chen, D. Davis, G. Huey, and D. Tanner (2004), Measurements of OH, HO$_2$+RO$_2$, H$_2$SO$_4$, and MSA at the South Pole during ISCAT 2000, *Atmos. Environ.*, *38*, 5423–5437, doi:10.1016/j.atmosenv.2004.06.031.

Mauldin, R. L., E. Kosciuch, F. L. Eisele, G. Huey, D. Tanner, S. Sjostedt, D. Blake, G. Chen, J. Crawford, and D. Davis (2010), South Pole Antarctica observations and modelling results: New insights on HO$_x$ radical and sulphur chemistry, *Atmos. Environ.*, *44*, 572–581, doi:10.1016/j.atmosenv.2009.07.058.

Mayer, B., and M. Degünther (2000), Comment on "Measurements of erythemal irradiance near Davis Station, Antarctica: Effect of inhomogeneous surface albedo," *Geophys. Res. Lett.*, *27*, 3489–3490, doi:10.1029/1999GL011171.

McKinlay, A. F., and B. L. Diffey (1987), A reference action spectrum for ultra-violet induced erythema in human skin, in *Human Exposure to Ultraviolet Radiation: Risks and Regulations*, edited by W. R. Passchler and B. F. M. Bosnajakovic, pp. 83–87, Elsevier, New York.

Penkett, S. A., P. S. Monks, L. J. Carpenter, K. C. Clemitshaw, G. P. Ayers, R. W. Gillett, I. E. Galbally, and C. P. Meyer (1997), Relationships between ozone photolysis rates and peroxy radical concentrations in clean marine air over the Southern Ocean, *J. Geophys. Res.*, *102*(D11), 12,805–12,817, doi:10.1029/97JD00765.

Pépy, G. (2011), Etude du formaldéhyde en zone côtière Antarctique, PhD thesis, 251 pp., Univ. Joseph Fourier de Grenoble, Grenoble, France.

Pommereau, J. P., and F. Goutail (1988), O$_3$ and NO$_2$ ground-based measurements by visible spectrometry during arctic winter and spring, *Geophys. Res. Lett.*, *15*, 891–894, doi:10.1029/GL015i008p00891.

Reiner, T., M. Hanke, and F. Arnold (1997), Atmospheric peroxy radical measurements by ion molecule reaction-mass spectrometry: A novel analytical method using amplifying chemical conversion to sulfuric acid, *J. Geophys. Res.*, *102*, 1311–1326, doi:10.1029/96JD02963.

Riedel, K., R. Weller, O. Schrems, and G. König-Langlo (2000), Variability of tropospheric hydroperoxides at a coastal surface site in Antarctica, *Atmos. Environ.*, *34*, 5225–5234, doi:10.1016/S1352-2310(00)00322-8.

Rohrer, F., and H. Berresheim (2006), Strong correlation between levels of tropospheric hydroxyl radicals and solar ultraviolet radiation, *Nature*, *442*, 184–187, doi:10.1038/nature04924.

Saiz-Lopez, A., A. S. Mahajan, R. A. Salmon, S. J.-B. Bauguitte, A. E. Jones, H. K. Roscoe, and J. M. C. Plane (2007), Boundary layer halogens in coastal Antarctica, *Science*, *317*(5836), 348–351, doi:10.1126/science.1141408.

Saunders, S. M., M. E. Jenkin, R. G. Derwent, and M. J. Pilling (2003), Protocol for the development of the Master Chemical Mechanism, MCM v3 (Part A): Tropospheric degradation of nonaromatic volatile organic compounds, *Atmos. Chem. Phys.*, *3*, 161–180, doi:10.5194/acp-3-161-2003.

Slusher, D. L., et al. (2010), Atmospheric chemistry results from the ANTCI 2005 Antarctic plateau airborne study, *J. Geophys. Res.*, *115*, D07304, doi:10.1029/2009JD012605.

Smith, S. C., J. D. Lee, W. J. Bloss, G. P. Johnson, T. Ingham, and D. E. Heard (2006), Concentrations of OH and HO$_2$ radicals during NAMBLEX: Measurements and steady state analysis, *Atmos. Chem. Phys.*, *6*, 1435–1453, doi:10.5194/acp-6-1435-2006.

Tanner, D. J., A. Jefferson, and F. L. Eisele (1997), Selected ion chemical ionisation mass spectrometric measurements of OH, *J. Geophys. Res.*, *102*(D5), 6415–6425, doi:10.1029/96JD03919.

Theys, N., et al. (2011), Global observations of tropospheric BrO columns using GOME-2 satellite data, *Atmos. Chem. Phys.*, *11*, 1791–1811, doi:10.5194/acp-11-1791-2011.

Walker, S. J., A. V. Jackson, M. J. Evans, J. B. McQuaid, and R. Salmon (2006), Assessment of hydrogen peroxide in the coastal Antarctic boundary layer, *Geophys. Res. Abstr.*, *8*, 03740.

Wang, Y., Y. Choi, T. Zeng, D. Davis, M. Buhr, L. G. Huey, and W. Neff (2007), Assessing the photochemical impact of snow NO$_x$ emissions over Antarctica during ANTCI 2003, *Atmos. Environ.*, *41*, 3944–3958, doi:10.1016/j.atmosenv.2007.01.056.

Zhu, R. B., Y. S. Liu, H. Xu, J. Ma, S. P. Zhao, and L. G. Sun (2008), Nitrous oxide emissions from sea animal colonies in the maritime Antarctic, *Geophys. Res. Lett.*, *35*, L09807, doi:10.1029/2007GL032541.

Zhu, R., Y. Liu, J. Ma, J. Sun, H. Xu, and L. Sun (2009), Greenhouse gas emissions from penguin guanos and ornithogenic soils in coastal Antarctica: Effects of freezing-thawing cycles, *Atmos. Environ.*, *43*, 2336–2347, doi:10.1016/j.atmosenv.2009.01.027.